DOI: 10.1002/asia.200800211

Pt^{II} Complexes with 6-(5-Trifluoromethyl-Pyrazol-3-yl)-2,2′-Bipyridine Terdentate Chelating Ligands: Synthesis, Characterization, and Luminescent Properties

Jing-Lin Chen,[a] Sheng-Yuan Chang,[a] Yun Chi,*[a] Kellen Chen,[a] Yi-Ming Cheng,[b] Chun-Wei Lin,[b] Gene-Hsiang Lee,[b] Pi-Tai Chou,*[b] Chen-Hao Wu,[c] Ping-I Shih,[c] and Ching-Fong Shu*[c]

Abstract: A series of Pt^{II} complexes Pt(fpbpy)Cl (**1**), Pt(fpbpy)(OAc) (**2**), Pt(fpbpy)(NHCOMe) (**3**), Pt(fpbpy)(NHCOEt) (**4**), and [Pt(fpbpy)(NCMe)](BF_4) (**5**) with deprotonated 6-(5-trifluoromethyl-pyrazol-3-yl)-2,2′-bipyridine terdentate ligand are prepared, among which **1** is converted to complexes **2**–**5** by a simple ligand substitution. Alternatively, acetamide complex **3** is prepared by hydrolysis of acetonitrile complex **5**, while the back conversion from **3** to **1** is regulated by the addition of HCl solution, showing the reaction sequence **1**→**5**→**3**→**1**. Multilayer OLED devices are successfully fabricated by using triphenyl-(4-(9-phenyl-9H-fluoren-9-yl)phenyl) silane (TPSi-F) as host material and with doping concentrations of **1** varying from 7 to 100%. The electroluminescence showed a substantial red-shifting versus the normal photoluminescence detected in solution. Moreover, at a doping concentration of 28%, the device showed a saturated red luminescence with a maximum external quantum yield of 8.5% at 20 mA cm^{-2} and a peak luminescence of 47543 cd m^{-2} at 18.5 V.

Keywords: charge transfer · chelates · N ligands · platinum · OLEDs

Introduction

Square-planar d^8-Pt^{II} complexes have attracted a great deal of interest because of their intriguing spectroscopic and photophysical properties, as well as their promising applications in optical-power limiting,[1] electroluminescence,[2] chemosensors,[3] anticancer medicine,[4] and photocatalysis.[5] These Pt^{II} complexes exhibit bright emission in solution, attributed to a combination of ligand-centered ππ* and metal-to-ligand charge transfer (MLCT) transitions.[6] Moreover, owing to the higher tendency in forming Pt···Pt and π···π interactions in the condensed phase, the respective emission often shows a clear red shift relative to the emission recorded in a dilute solution. These transitions are often denoted as either metal–metal-to-ligand charge transfer (MMLCT)[7] or excimeric ligand-to-ligand charge transfer emission.[8]

Among the chelating ligands documented in the literature, 2,2′-bipyridine (Figure 1) is the most popular neutral ligand, and it can interact with a metal atom using simple dative bonding involving N-donor atoms. On the other hand, 2-phenylpyridine is known for its capability of undergoing a cyclometalation reaction, by supplying the anionic bonding character with respect to the central metal atom.[9] In sharp contrast, C-linked 2-pyridyl azoles, such as pyrazoles, are known to serve as both neutral chelating ligands[10] or anionic chelates by deprotonation of the pyrazolyl-NH bond.[11] The latter process is conceptually related to the cyclometalation. In fact, these functionalized C-linked 2-pyridyl pyrazoles have served as excellent candidates in stabilizing and

[a] Dr. J.-L. Chen, S.-Y. Chang, Prof. Y. Chi, K. Chen
Department of Chemistry
National Tsing Hua University
Hsinchu 30013 (Taiwan)
Fax: (+886) 3-572-0864
E-mail: ychi@mx.nthu.edu.tw

[b] Dr. Y.-M. Cheng, C.-W. Lin, Dr. G.-H. Lee, Prof. P.-T. Chou
Department of Chemistry and Instrumentation Center
National Taiwan University
Taipei 10617 (Taiwan)
Fax: (+886) 2-2369-5208
E-mail: chop@ntu.edu.tw

[c] C.-H. Wu, P.-I. Shih, Prof. C.-F. Shu
Department of Applied Chemistry
National Chiao Tung University
Hsinchu 30010 (Taiwan)
E-mail: shu@cc.nctu.edu.tw

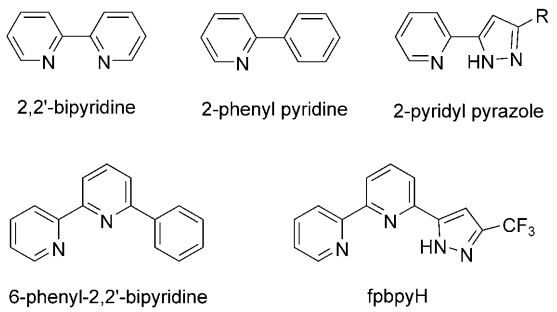

Figure 1. Chemical structures of some common chelating ligands.

fine-tuning the chemical and photophysical properties of metal complexes.[12]

Parallel to the chemistry of bidentate cyclometalating chelates, 6-phenyl-2,2′-bipyridine is probably the most widely investigated terdentate cyclometalating ligand for stabilization of the Pt^{II}–metal framework.[13] Significant study has also been related to the system involving symmetrical 1,3-di(2-pyridyl)-benzene, for which the cyclometalated ligand is located at the central position of the terdentate ligand.[14] Encouraged by the success of these attempts, we decided to focus on distinctive bidentate chelates, such as 2-pyridyl pyrazole,[15] and terdentate ligands, like 6-(5-trifluoromethyl-pyrazol-3-yl)-2,2′-bipyridine, denoted as fpbpyH.[16] It is noted that the electron-withdrawing CF_3 substituent of fpbpyH not only increases the pyrazolic N–H acidity and activity, but also minimizes the unwanted side reaction by blocking coordination to the adjacent nitrogen atom, allowing a stable and designated terdentate bonding. The resulting tailor-made ligand environment would then render extensive stabilization to the Pt^{II} complexes with the general formula Pt(fpbpy)X, in which X is an anionic or neutral ligand.

In this study, we focused on the preparation, characterization, and potential OLED application of a series of Pt^{II} complexes derived from Pt(fpbpy)Cl (**1**). As shown in Scheme 1, Pt^{II} complexes **2**, **3**, and **4** can be isolated by simple substitution of the chloride in **1** by acetate, acetamide, and propionamide, respectively. Intriguing photophysical properties of complexes **1**, **2**, and **3**, in both solution and solid phases were investigated. Moreover, the acetamide complex **3** can be obtained by in-situ hydrolysis of acetonitrile complex **5** in basic media, and the release of acetamide by back-conversion to **1** upon addition of dilute HCl solution. This pattern of reactivity also revealed one additional case for the metal-catalyzed hydrolysis of acetonitrile to acetamide. As a result, the reaction sequence documented here can serve as a useful mechanistic model for the Pt^{II}-catalyzed hydrolysis of organonitriles.[17] Finally, bright luminescence of **1** in the solid state has also encouraged us to utilize this material as a dopant for the fabrication of red-emitting phosphorescent organic light-emitting diodes (OLED)s.

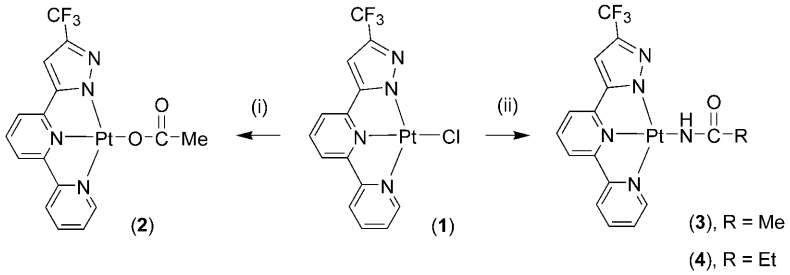

Scheme 1. Schematic for Pt^{II} complexes **2**, **3**, and **4** isolated by simple substitution of the chloride in **1** by acetate, acetamide, and propionamide, respectively. i) AgOAc in DMF, 100°C, ii) NH_2COR (R = Me or Et), Na_2CO_3 in ethanol, reflux.

Abstract in Chinese:

本文報導一系列含有去質子化的三牙螯合配位基 6-(5-trifluoromethyl-pyrazol-3-yl)-2,2'-bipyridine 鉑金屬錯合物 1–5。錯合物 1 可經由簡單的配位基取代反應轉換為錯合物 2–5。乙氰配位的錯合物 5 藉由水解反應可得錯合物 3，而錯合物 3 在鹽酸的作用下可轉換為錯合物 1，顯示錯合物之間有 1 → 5 → 3 → 1 的轉換關係。光物理方面，錯合物 3 在溶液中表現出不受濃度變化影響的紅色磷光（604 nm）。然而，錯合物 1 的溶液放光卻容易受濃度變化影響，證實其分子間有強的 Pt-Pt 作用力存在。晶體結構也顯示短的 Pt-Pt 距離（3.385 Å）。錯合物 1 在單晶型態具有強的磷光放光（675 nm），其對應的量子效率和壽命分別為 0.2 和 113 ns，主要是由分子間堆疊作用造成。以 TPSi-F 作主體材料，改變錯合物 1 的摻雜濃度以 7% 到 100%，製作了一系列多層結構的 OLED 元件。隨著摻雜濃度的增大，元件的放光也表現紅位移。最佳元件表現為摻雜濃度 28%，其最大外部量子效率和亮度分別為 8.5%（20 mA/cm²）與 47543 cd/m²（18.5 V）的飽和紅色磷光。

Results and Discussion

Synthesis and Characterization

The required terdentate chelate fpbpyH was obtained by a Claisen condensation reaction employing 6-acetyl-2,2′-bipyridine and ethyl trifluoroacetate, followed by treatment with an excess of hydrazine hydrate in refluxing ethanol according to procedures reported in the literature.[16,18] This ligand has a high potential for forming the anionic tridentate chelate by facile deprotonation during the reaction with a transition-metal reagent in basic media.

The key starting material, that is, complex **1**, was synthesized by heating the fpbpyH ligand and K_2PtCl_4 reagent in a 1:1 mixture of acetonitrile and water. Single red crystals were obtained by cooling the saturated mixture in DMSO and acetone. Its molecular composition was initially confirmed by the detection of all aromatic fpbpy signals in the ^1H NMR spectrum. Moreover, the addition of concentrated

HCl to **1** failed to protonate the noncoordinated pyrazolyl-nitrogen atom on **1**. This result is in sharp contrast to the related bidentate ligands, 2-pyridyl pyrazole and 1-isoquinolinyl indazole, which are capable of forming Pt^{II} complexes with the neutral chelating ligand.[19]

Crystal structural analysis shows that complex **1** adopts a distorted square-planar geometry as shown in Figure 2. The N–Pt–N bond angles, N(1)–Pt–N(2) = 80.0(4)°, N(2)–Pt–N(3) = 80.6(4)°, N(1)–Pt–N(3) = 160.6(3)° (see Table 1) deviate slightly from the idealized values of 90° and 180° as a consequence of the internal constraint imposed by the fpbpy ligand. These results are common for Pt^{II} complexes with a terdentate-cyclometalated chelate.[20] All the Pt–N bond distances, Pt–N(1) = 2.025(9) Å, Pt–N(2) = 1.931(9) Å, and Pt–N(3) = 1.987(9) Å, are comparable to those found in other Pt^{II} complexes possessing a bipyridyl group.[21] The central Pt–N distance of the ligand fpbpy is shorter than those of the outer nitrogen atoms, mainly because of the steric demand as documented in the literature.[18] The Pt–Cl(1) distance of 2.314(3) Å is comparable to that of the other Pt^{II}-chloride complexes.[22] Furthermore, complex **1** exhibited a head-to-tail stacking along the *b* axis of the crystal lattice, giving a zigzag $[Pt]_n$ metal chain with intermolecular Pt···Pt distances of 3.385 Å and a Pt–Pt–Pt angle of 153.59°. This stacking pattern is similar to those observed in other linear-chain Pt^{II} complexes that show intermolecular Pt···Pt interaction and strong π···π stacking.[23] However, there is a reduced degree of π···π stacking between the fpbpy ligands in **1** arising from the alternating arrangement of this chelate.

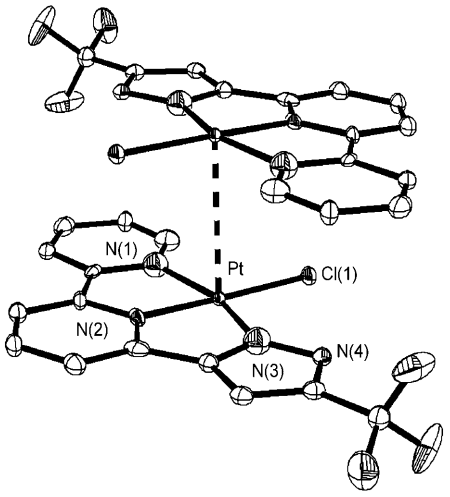

Figure 2. ORTEP drawing of **1** showing atom-labeling scheme with 30% thermal ellipsoids and the Pt···Pt interaction in the crystal lattices.

Table 1. Selected bond length (Å) and angles (°) for complexes **1** and **3**.

Complex **1**			
Pt–N(1)	2.025(9)	Pt-N(2)	1.931(9)
Pt–N(3)	1.987(9)	Pt-Cl(1)	2.314(3)
Pt···Pt	3.385		
N(2)–Pt–N(1)	80.6(4)	N(2)-Pt-N(3)	80.0(4)
N(1)–Pt–Cl(1)	97.5(3)	N(3)-Pt-Cl(1)	102.0(3)
N(3)–Pt–N(1)	160.6(3)	N(2)-Pt-Cl(1)	178.0(3)
Complex **3**			
Pt(1)–N(1)	2.043(6)	Pt(1)–N(2)	1.951(6)
Pt(1)–N(3)	1.996(5)	Pt(1)–N(5)	2.012(6)
Pt(1)···Pt(1)	4.587	4.968	
N(2)–Pt(1)–N(1)	79.9(2)	N(2)–Pt(1)–N(3)	80.4(2)
N(5)–Pt(1)–N(1)	104.2(2)	N(3)–Pt(1)–N(5)	95.5(2)
N(3)–Pt(1)–N(1)	160.3(2)	N(2)–Pt(1)–N(5)	173.5(2)

Reactivity studies showed that treatment of **1** with silver acetate resulted in the formation of the acetate-substituted derivative **2**, for which the Ag^+ cation served as the chloride scavenger, allowing the acetate to occupy the fourth coordination site of the Pt^{II} cation. Similarly, treatment of **1** with acetamide or propionamide in the presence of Na_2CO_3 afforded the respective amido complexes **3** and **4** in refluxing ethanol solution. Additional support was given by the ^1H NMR spectral analysis, from which the detection of methyl and ethyl signals for **3** and **4** confirmed their existence, while the unique NH proton of the acetamide ligand occurred at δ 5.58 (**3**) and δ 5.60 (**4**), which are within the ^1H NMR spectral range (δ 4.99–5.78) reported for other Pt^{II}–acetamide complexes.[24]

The single crystals of **3** could be obtained by slow cooling of the supersaturated solution in DMSO to room temperature. The solid-state structure of **3** is studied by X-ray diffraction analysis. Figure 3 shows only one crystallographically independent molecule in the asymmetric unit. As shown

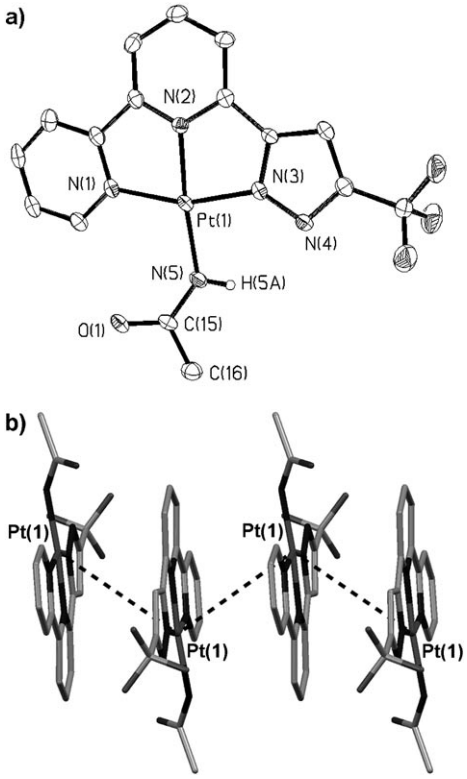

Figure 3. (a) ORTEP drawing of one crystallographic independent molecule of **3** with 30% thermal ellipsoids, and (b) the side view that depicted the accompanying packing diagram in the crystal lattices.

in Table 1, all metrical parameters are very similar to those of **1**, which shows virtually identical Pt–N bond distances, as well as closely related bite angles, to the fpbpy ligand, while the accompanying $Pt–N_{acetamide}$ distances occur in the range of 2.012(6)–2.010(6) Å, which are comparable to those of the Pt^{II}–amidate complexes reported.[25] Moreover, **3** exhibited head-to-tail and zigzag stacking along the *a* axis, with two pairs of alternating Pt···Pt nonbonding distances (3.569 and 5.683 Å for distances between Pt(2) atoms, and 4.587 and 4.968 Å for distances between Pt(1) atoms) which are significantly longer than that of **1**, but are akin to those observed in other stacked Pt^{II} complexes.[26] It is notable that the shortest Pt–Pt distance in **3** is far longer than the theoretical limit of 3.5 Å, which is the maximum distance for effective overlap between Pt-d_z^2 and -p_z orbitals. As a result, complex **3** showed the existence of only weakly bonded dimers, if there is such nonbonding interaction at all in the solid state. On the other hand, in sharp contrast to that of **1**, the fpbpy chelate of each Pt molecule exhibits a favorable side-to-side stacking with one another (see Figure 3b). The inter-planar distances are estimated in the range of 3.3–3.5 Å, which is below the upper limit of 3.8 Å for typical π···π interactions detected for aromatic compounds.[27]

It is worthwhile to note that the chloride complex **1** reacted slowly with Na_2CO_3 in refluxing acetonitrile. The suspension first turned into a transparent solution, showing the depletion of the starting material and the formation of some soluble intermediate. Then, a trace amount of precipitate began to deposit from the solution. The result is consistent with the sequential conversion from the intermediate, which is highly soluble in acetonitrile, to the less soluble acetamide complex **3**. Finally, the solution turned into a turbid yellow suspension, which showed the complete formation of the end product **3**. For further investigation and confirmation of this stepwise transformation, reaction of **1** with one equiv of $AgBF_4$ in anhydrous acetonitrile was conducted. A highly soluble, orange–yellow complex identified as the acetonitrile complex [Pt(fpbpy)(NCMe)](BF_4) **5** was afforded. Complex **3** is attainable by treatment of **5** with a slight excess of Na_2CO_3 in mixed acetonitrile and water, confirming the status of **5** as the intermediate for the aforementioned transformation of **1** to **3** (Scheme 2). For the final confirmation, the propionamide complex **4** was also accessible by treatment of **1** with $AgBF_4$, followed by the addition of both propionamide and Na_2CO_3 in DMF at elevated temperature, while both **3** and **4** could be reverted to **1** by treatment with HCl (2 M) upon reflux, showing the sequential ligand transformation from chloride, nitrile, acetamide, and back to the chloride.

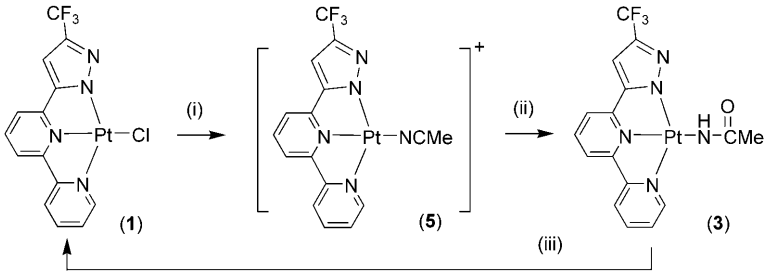

Scheme 2. Schematic for complex **3** obtained by treatment of **5** with slight excess of Na_2CO_3 in mixed acetonitrile and water. i) $AgBF_4$ in MeCN, reflux; ii) Na_2CO_3 in MeCN/H_2O, reflux; iii) 2 M $HCl_{(aq)}$.

Photophysical Properties

The UV/Vis absorption and emission spectra of complexes **1**, **2**, and **3** in CH_2Cl_2 at 298 K are shown in Figure 4. All pertinent spectroscopic data are tabulated in Table 2. To gain further insight into the photophysical behavior of all titled complexes, density functional theory (DFT) was also applied to access molecular-orbital information. As a result, those HOMO and LUMO that are mainly involved in the lowest-lying transition are depicted in Figure 5 and the description of the energy gap of each transition is listed in Table 3. It has been noticed that TDDFT (time-dependent density functional theory) yields substantial errors for the excitation energies of charge-transfer excited states, when local functionals, such as LDA or GGA, are used.[28] Nevertheless, it has been widely recognized as an efficient method to explore the electronic structures of certain organometallic complexes. Furthermore, the continuum-solvation model of CH_2Cl_2 (IEFPCM) used in this approach might also contribute to some errors, which leads to a further deviation of the results obtained from the calculations as compared to those from experiment. However, after a qualitative comparison of Tables 2 and 3, the calculated energy gaps agree satisfactorily with the experimentally obtained photophysical data, suggesting that the TDDFT calculations are able to predict the photophysical behavior of these Pt^{II} complexes to a certain degree.

For complex **1**, there are several absorption bands ranging from 250–370 nm with intense molar extinction coefficients $\varepsilon > 10^4\,M^{-1}cm^{-1}$ and a relatively weaker transition ($\varepsilon \sim 2.4 \times 10^3\,M^{-1}cm^{-1}$) at longer wavelengths (maximized at ~400 nm). With reference to previous work on Pt^{II} complexes possessing the C^N^N and N^N^N terdentate ligands,[22,29] the absorptions at 250–370 nm most likely originate from the ligand-centered $^1\pi\pi^*$ transitions. Further support is given by the close matching of several absorption bands in the high-energy region ($\leq$370 nm) in complexes **1**, **2**, and **3** with the same ligand, fpbpy. Moreover, as shown in the highest occupied and lowest unoccupied molecular orbitals (HOMO and LUMO) of complex **1** (see Figure 5), the electron density shifted from the central metal ion to the ligands, indicating a metal-to-ligand charge transfer (MLCT) transition of the lowest singlet transition. Also, the MLCT character for the lowest singlet transition of **1** was calculated to be 20.9% (see Table 3). Therefore, the

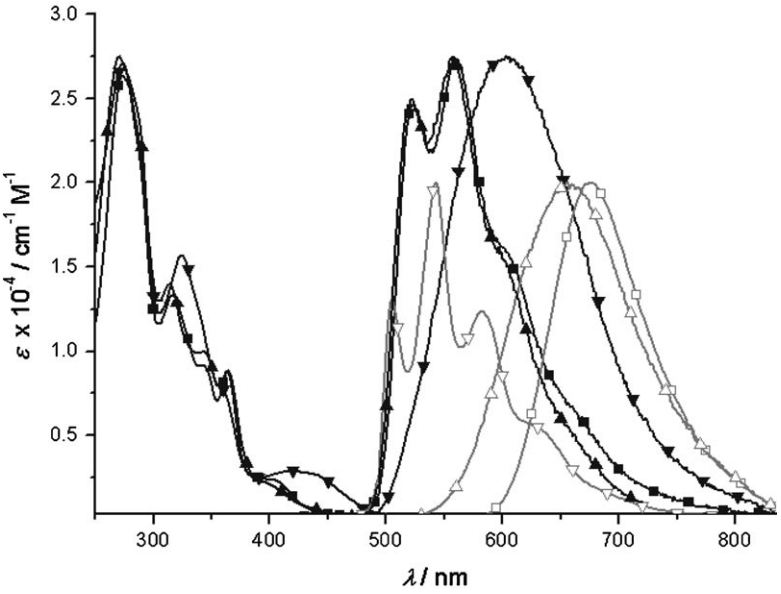

Figure 4. UV/Vis absorption and emission spectra of **1** (-■-), **2** (-▲-), and **3** (-▼-) recorded in a dilute CH_2Cl_2 solution at RT (see text). The gray lines with the open symbols (-□-△-▽-) depicted the emission spectra of the respective single crystal samples. Note that the emission intensity is in arbitrary units.

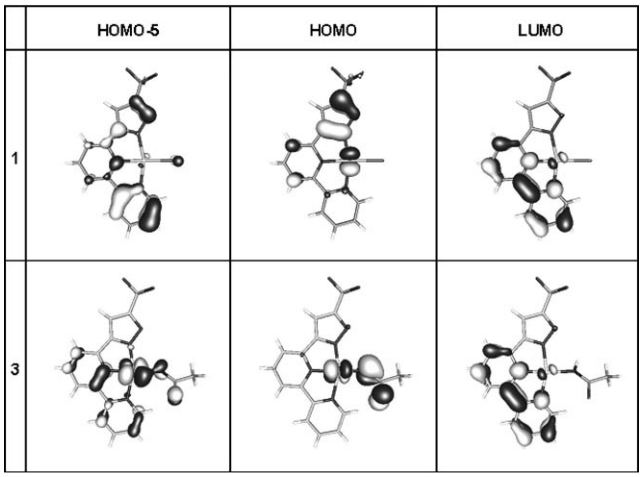

Figure 5. The HOMO and LUMO for Pt^{II} complexes **1** and **3**.

broad-band absorption at ~400 nm can be reasonably assigned as the metal-to-ligand charge transfer transition (^{1}MLCT) from the d_π orbital of the ($5d^8$) Pt-metal center to the unoccupied π* orbital of the ligand (fpbpy), mixed with the intra-ligand ππ* transition inside fpbpy. The frontier orbitals of the HOMO and LUMO in complex **2** (not shown here) are essentially similar to that of **1**. This can be further supported by the closely matched absorption and emission spectra between **1** and **2**. Accordingly, for **2**, the strong absorption bands (≤370 nm) are thus assigned to the ligand-centered ^{1}ππ* transitions, and the comparatively weak absorption at around 410 nm is attributed to the ligand-centered ^{1}ππ* transitions mixed with a certain degree of MLCT. On the same basis, the intense absorption bands of **3** at 250–370 nm can thus be assigned as the intra-ligand ^{1}ππ* transitions of the fpbpy ligand. Moreover, the relatively weaker absorption at 418 nm can be attributed to the spin-allowed ^{1}MLCT transitions (17.5%) mixed with the ligand-centered ππ* transition (see Table 3). However, it is interesting to note that the predominant ligand-centered ππ* transition is ascribed to an inter-ligand charge transfer transition from acetamide to the bipyridyl fragment of fpbpy ligand according to the result from the molecular-orbital analyses (see Figure 5).

In a dilute solution of CH_2Cl_2, **1** (8.46×10^{-6} M), **2** (7.33×10^{-6} M), and **3** (9.0×10^{-6} M) exhibited emission with a peak wavelength at 560 nm, 557 nm, and 604 nm, respectively. The radiative rate constant (k_r) is defined by $k_r = k_{obs}\times\Phi_{em}$, in which, k_{obs} and Φ_{em} denote the observed decay rate constant and emission quantum yield, respectively. Accordingly, by using the data listed in Table 2, k_r is calculated to be $7.5\times10^4\ s^{-1}$ for **1**, $1.1\times10^4\ s^{-1}$ for **2**, and $4.4\times10^4\ s^{-1}$ for **3**. This result leads to the unambiguous confirmation that the emission is phosphorescence. The theoretical calculation also showed satisfying results in predicting the T_1–S_0 transition gap of **1**, which closely fits the emission band, with 19.4% MLCT character (see Table 3). However, with regard to the spectral features, complexes **1** and **2** revealed emission with

Table 2. UV/Vis absorption and emission data of **1** and **3** in CH_2Cl_2 at RT.

	Abs λ_{max} [nm] ($\varepsilon\times10^{-3}$ M^{-1}cm^{-1})	Em λ_{max} [nm]	τ [ns]	Φ_{em}	k_r
1	273 (26.4), 317 (13.3), 343 (9.2), 363 (8.8), 400 (2.4)	524, 560 (675)[a]	173 (113)[b]	1.3×10^{-2} (0.2)[b]	7.3×10^4 (1.7×10^6)[b]
2	270 (27.5), 314 (14.0), 343 (10.0), 365 (8.9), 400 (2.1)	522, 557 (656)[a]	187 (26.0)[a]	2.1×10^{-3} (–)[c]	1.1×10^4
3	274 (27.1), 324 (15.7), 418 (2.9)	604 (505, 543, 582, 636)[a]	2.45 (292)[a]	1.0×10^{-2} (–)[c]	4.4×10^4

[a] The data in the parentheses are obtained from the single crystalline samples. [b] The solid-state photophysical data of **1** was measured using a vacuum-deposited thin film sample. [c] Sample decomposed during preparation of thin film.

Table 3. The calculated energy levels and orbital-transition analyses of **1** and **3** in the continuum-solvation model of CH_2Cl_2 (IEFPCM model, see Experimental Section).

	State	λ_{cal} [nm]	f	Assignment	MLCT %
1	T_1	512.9		HOMO→LUMO (93%)	19.4
				HOMO-5→LUMO (7%)	
	S_1	448.4	0.0022	HOMO→LUMO (88%)	20.9
				HOMO-1→LUMO (6%)	
3	T_1	519.8		HOMO→LUMO (95%)	19.8
				HOMO-5→LUMO (5%)	
	S_1	465.4	0.0342	HOMO→LUMO (93%)	17.5

notable vibronic progressions as opposed to a featureless pattern in **3**, despite complexes **1**–**3** all possessing the same fpbpy ligand and a similar MLCT percentage at the triplet manifold, that is, 19.4% for **1**, 18.5% for **2**, and 19.8% for **3**. This drastic difference again evidenced the intrinsic differences in their frontier orbitals, being intra-ligand for **1** and **2** versus inter-ligand charge transfer for **3**, involved in the lowest lying transition.

As for the red-shifted lowest lying absorption of **3** with respect to **1** and **2**, one plausible explanation might lie in the difference in bonding strength of the chloride or acetate versus acetamide to the central Pt^{II} cation. The anion could probably contribute its electron densities to the d orbital of the central Pt^{II}-metal ion, leading to a stronger dative interaction. Consequently, the orbital energy of the central Pt^{II} ion could be increased arising from the conveying of electron density from this anion, and thereby decreasing the electron-transition gap. Accordingly, the donor strength of acetamide in **3** is believed to be stronger than that between the chloride (acetate) and Pt^{II} in **1** (or **2**), resulting in a smaller energy gap in **3**.

It is also believed that the π-conjugation may also play a certain role to account for the red-shifted emission of **3** with respect to **1** and **2**. As shown in Figure 5, for **3**, the frontier orbitals have been extensively extended to the acetamide. Particularly, both the HOMO-5 and HOMO in **3** clearly indicate the involvement of the nitrogen and the carbonyl group of acetamide. With such an enlarged conjugated π system, the HOMO–LUMO gap decreases, such that the emission of **3** is red-shifted with respect to **1**. For further confirmation, Figure 6 depicts a plot of the partial density of states, in which the contributions of different moieties to specific frontier orbitals are illustrated. The large percentage of the acetamide contribution in the HOMO assures its pivotal role in the ππ* transition, and renders firm support for its photophysical properties. As for complex **1** (or **2**), the electron-density distribution in the HOMO (see Figure 5) indicates nearly no participation of the chloride (or acetate, not shown here because of the similarity) to the overall conjugated system. As a result, its influence to the electron density of the Pt^{II} ion is apparently smaller than that in **3**. Accordingly, Figure 6 further illustrates the reduced electron-density contribution of the chloride to the HOMO.

As shown in Figure 7, the emission profile of **1** exhibits apparent concentration dependences. Upon increasing the

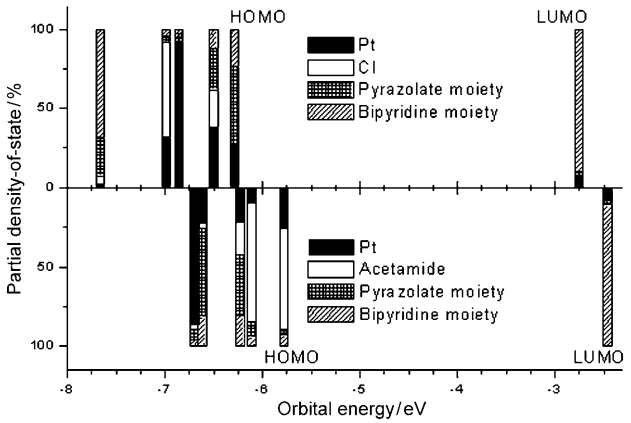

Figure 6. The spectrum of partial density-of-states of complexes **1** (upper) and **3** (bottom).

concentration of **1** in CH_2Cl_2 from 8.46×10^{-6} M to 1.21×10^{-4} M, in addition to the ~560 nm emission peak (defined as the F_1 band), a lower energy emission band maximum at ~660 nm (defined as the F_2 band) gradually increases, accompanied by a decrease of the F_1 band. The excitation spectra monitored at either F_1 (e.g., 520 nm) or F_2 band (e.g., 700 nm) are identical to each other (not shown here) and to the absorption spectrum, indicating that both emission bands originate from the same ground-state species. Knowing there exists a higher tendency for forming multiple Pt···Pt interactions in the condensed phase, it is thus reasonable to ascribe the F_2 band to originate from either metal–metal-to-ligand charge transfer (MMLCT)[7] or excimeric ligand-to-ligand charge transfer emission.[8] Further evidence is given by the emission spectrum of **1** recorded using a single-crystal sample (see the Experimental Section). Complex **1** exhibits a well-aligned head-to-tail stacking along the *b* axis of crystal lattices, with intermolecular Pt···Pt distances

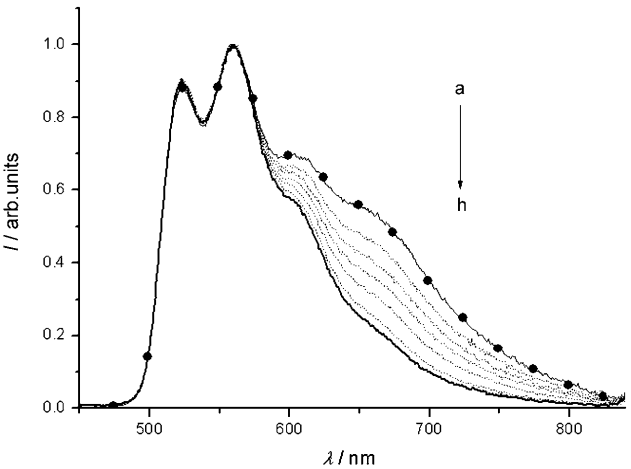

Figure 7. The emission spectra of **1** excited at 284 nm in CH_2Cl_2 solution at RT by varying the concentrations from (a) 1.21×10^{-4} M (-●-), (b) 9.63×10^{-5} M, (c) 7.20×10^{-5} M, (d) 5.76×10^{-5} M, (e) 4.43×10^{-5} M, (f) 2.23×10^{-5} M, (g) 1.15×10^{-5} M, and (h) 8.46×10^{-6} M (solid line). All emission spectra are normalized at 565 nm.

as short as 3.385 Å (as mentioned previously). As a result, **1** as a single-crystal sample illustrated a stacking perturbed emission maximum at 675 nm, the peak of which is consistent with that of the excimeric-like emission, that is, the F_2 band of 660 nm, for a solution of **1** in CH_2Cl_2. The concentration-dependent emission features have also been observed in **2** (not shown here), supporting its similar stacking framework as that of complex **1**. Conversely, in the case of **3**, the emission feature remained unchanged up to 1×10^{-4} M in CH_2Cl_2. This can plausibly be rationalized by the relatively small tendency for self-association in **3**, as it forms only dimers in the crystal lattices (see Figure 3), while complex **1** (or **2**) showed strong aggregation to afford the $[Pt]_n$ long-chain arrangement. Thus, as opposed to the largely red-shifted emission of **1** (the F_2 band) in crystal versus that observed in CH_2Cl_2 solution (the F_1 band), the emission of **3** in solid crystal revealed a slightly blue-shifted emission (as compared to the emission in solution), possessing notable vibronic progression possibly caused by the space confinement, that is, the rigidity of molecular geometry.

To gain more insights into the excimer formation, the relaxation dynamics of monomer and excimer were obtained for an aerated solution of **1** in CH_2Cl_2 (1.1×10^{-4} M). By monitoring the emission at 500 nm, the lifetime of monomer is fitted to a single exponential to give a decay of ~126 ns, while the relaxation of the excimer monitored at 700 nm is composed of a rise and decay component of 112 ns and 117 ns, respectively. The rise component, considering the uncertainty arising from the spectral fitting, is the same as the decay of the monomer. This result firmly supports the precursor–successor relationship between the monomer and the excimer in the excited state.

Furthermore, assuming that the concentration of **1** in the excited state is relatively small when compared to that of the ground state, the mechanism of excimer formation can be expressed using a pseudo first-order approximation:

$$A^* \xrightarrow{k_1[A]} (A-A)^* \xrightarrow{k_3} A + A \quad (1)$$

$$A^* \xrightarrow{k_2} A \quad (2)$$

Thus, the time-dependent concentrations of excited monomer, A^*, and excimer, $(A{-}A)^*$, can be expressed as

$$A^*(t) = A^*(0)\cdot\exp(-(k_1[A]) + k_2) \quad (3)$$

$$(A-A)^*(t) = \frac{k_1[A]A^*(0)}{k_1[A]+k_2+k_3}(\exp(-k_3 t) - \exp(-(k_1[A]+k_2))t) \quad (4)$$

where k_1 denotes the bimolecular rate constant of excimer formation, k_2 stands for the overall relaxation rate constant except for the contribution from excimer formation, and k_3 represents the relaxation rate constant of excimer. Note that Equation (1) was derived under the assumption that the reverse process involving $(A{-}A^*)\rightarrow A^*+A$ is energetically prohibited.

As a result, the plot of observed decay rate constant of the excited monomer (A^*) as a function of concentration [A] reveals a straight line (see Figure 8). This result is expected because the observed decay rate constant of the monomer, in theory, is the sum of $k_1[A]+k_2$ [Eq. (3)]. The slope and intercept are then deduced to be $7.2\times10^{10}\,M^{-1}s^{-1}$ (k_1) and $7.1\times10^6\,s^{-1}$ (k_2), respectively.

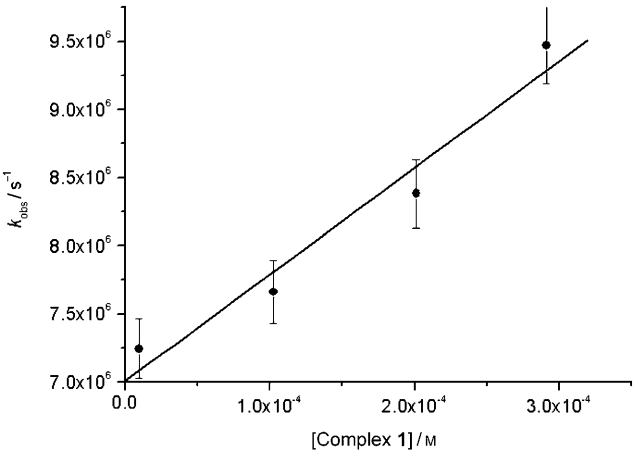

Figure 8. The plot of observed decay rate constant of excited monomer **1** as a function of the concentration. The slope and intercept of the fitted results are 7.2×10^9 and 7.1×10^6, respectively.

The efficiency of the excimer formation, Φ_{eff}, is defined as:

$$\Phi_{eff} = \frac{k_1[A]}{k_{obs}} \quad (5)$$

With the known emission quantum yield, Φ_{mon}, of monomeric **1**, the emission quantum yield of the excimer, Φ_{ex}, can be expressed as:

$$\Phi_{ex} = \Phi_{mon}\frac{(1-\Phi_{eff})\cdot I_{ex}}{\Phi_{eff}\cdot I_{mon}} \quad (6)$$

where I_{mon} and I_{ex} denote the integrated emission intensity of excited monomer and excimer, respectively.

As a simple approach, by knowing k_1, k_{obs} (monomer), and for example, $[A]=1.1\times10^{-4}$ M, Φ_{eff} is then calculated to be 10.6%. Φ_{mon} has been determined to be 0.01 in dilute solution (see Table 2). Under $[A]=1.1\times10^{-4}$ M, the deconvoluted I_{ex}/I_{mon} is calculated to be 0.28. As a result, Φ_{ex} is deduced to be 2.3%. The observed rate constant for the excimer emission is measured to be $8.5\times10^6\,s^{-1}$. Therefore, the radiative decay rate constant of the excimer emission is deduced to be $2.0\times10^5\,s^{-1}$ and is larger than that ($7.3\times10^4\,s^{-1}$) of the monomer emission. This result is fundamentally intriguing, indicating that the contribution of the metal-d_π orbital increases upon excimer formation. Theoretically, this can be rationalized by the formation of Pt^{II}–Pt^{II} d_{z^2} interaction in the excited state, resulting in a raise of the d_{z^2} energy

level (HOMO), and hence the reduction of the energy gap, as well as the increase of the MLCT contribution. This proposed mechanism is consistent with the packing arrangement of **1** revealed in the single crystal, in which the π stacking between two adjacent complexes is obscure in comparison to the major Pt^{II}–Pt^{II} interaction.

OLED Fabrication

The Pt^{II} complex **1** exhibits excellent thermal stability and good phosphorescence efficiency, which are desirable for light-emitting diode applications. To study the device performances of **1**, the multilayer devices of the configuration ITO/NPB(30 nm)/mCP(10 nm)/TPSi-F:**1**(40 nm)/BCP-(10 nm)/TPBI(30 nm)/LiF(1 nm)/Al(100 nm) were prepared. The abbreviations NPB, mCP, TPSi-F, BCP, and TPBI stand for 4,4′-bis(*N*-(1-naphthyl)-*N*-phenylamino)biphenyl, 1,3-bis(9-carbazolyl)benzene, triphenyl-(4-(9-phenyl-9*H*-fluoren-9-yl)phenyl) silane,[30] 2,9-dimethyl-4,7-diphenyl-1,10-phenanthroline, and 1,3,5-tris(*N*-phenyl benzimidazol-2-yl)benzene, respectively, while doping concentrations of **1** are 7%, 14%, 28%, 50% and 100%. Very bright emission was observed for all doping concentrations. Table 4 summarizes the selected performance data for these OLED devices. The *I-V-L* curves, plotted in Figure 9, show a trend of increasing current density with increasing concentration of **1**. This phenomenon implies that the charges may be injected directly to the Pt^{II} complex; the dopant then serves as an additional channel to transport charges by hopping between the dopant sites.[31]

Figure 10a shows the electroluminescence (EL) emission profiles at various doping concentrations. The relative intensity of the peaks at 528 and 572 nm decreases with increasing concentrations. At the same time, the peak intensity at higher wavelengths increases. According to the previous photoluminescence (PL) data, it appears to us that the luminescence at 528 and 572 nm is derived from the monomeric species, while the emission at the longer wavelengths originates from the aggregated forms and/or excimers. Arising from the reduction of the monomeric species at the higher concentrations, the full width at half maximum (FWHM) of the EL signal decreased from 153 nm to 107 nm.

For a further comparison, the thin film samples of **1** doped in TPSi−F were prepared and their PL characteristics measured. The concentration dependent red-shifting was also displayed in the corresponding PL spectra (Figure 10b),

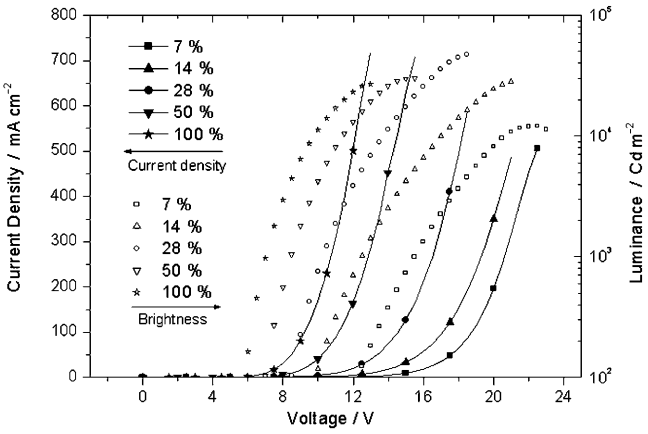

Figure 9. *I-V-L* characteristics of OLED devices ITO/NPB/mCP/TPSi-F:**1**/BCP/TPBI/LiF/Al as a function of dopant concentration.

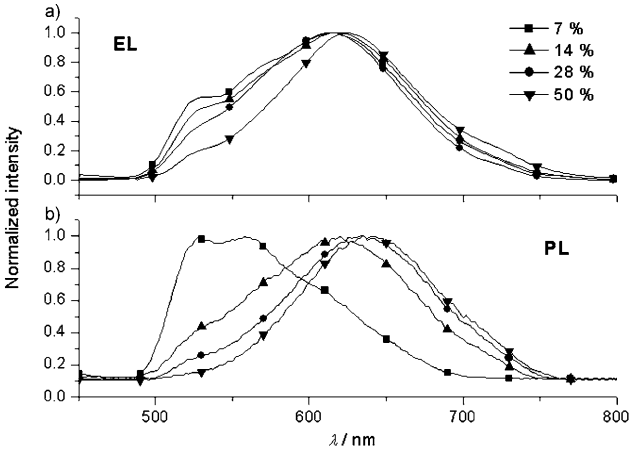

Figure 10. (a) EL spectra of OLED devices ITO/NPB/mCP/TPSi-F:**1**/BCP/TPBI/LiF/Al as a function of dopant concentration, and (b) PL spectra of **1** embedded to the TPSi-F matrix with variable dopant concentrations.

further substantiating the self-aggregation of the dopant. This tendency has been illustrated by the well-aligned head-to-tail stacking arrangement and the exceedingly short intermolecular Pt···Pt distances of **1**. In fact, the phenomenon is typical for the square-planar Pt^{II} complexes, for which intermolecular π···π and Pt···Pt interactions often result in molecular stacking and the formation of aggregates and excimers.[32] Therefore, the detected luminescence would display features involving both ^{3}MLCT and ^{3}MMLCT excited states, which are generated from the monomer and the oligomeric counterparts, respectively.[20b,33]

Moreover, among the various dopant concentrations, the best device was achieved at the 28 wt% doping level (Figure 11), which rendered a turn-on voltage of 6.7 V (at

Table 4. Performance characteristics for ITO/NPB/mCP/TPSi-F:**1**/BCP/TPBI/LiF/Al.

Conc. (%)	Max lum.[a] [cd m^{-2} (V)]	E.Q.E. [%][b]	Luminous eff. [cd A^{-1}][b]	Power eff. [lm W^{-1}][b]	E. L. λ_{max} (C.I.E.)[c]
7%	12021 (22.5)	3.3 (2.4)	6.9 (5.1)	1.4 (0.9)	530, 618 (0.50, 0.46)
14%	28289 (21.0)	6.6 (4.9)	13.8 (10.3)	3.1 (1.9)	530, 618 (0.52, 0.47)
28%	47543 (18.5)	8.5 (6.7)	18.5 (14.6)	4.9 (3.2)	530, 618 (0.53, 0.46)
50%	30056 (15.5)	7.6 (5.5)	11.4 (9.0)	3.9 (2.5)	532, 626 (0.56, 0.42)
100%	26888 (13.0)	6.5 (4.9)	10.1 (7.6)	4.2 (2.6)	630 (0.59, 0.41)

[a] Values in the parentheses are the applied driving voltage. [b] Data collected under 20 mA cm^{-2}, while values in the parentheses are the data collected under 100 mA cm^{-2}. [c] Measured at the driving voltage of 8 V.

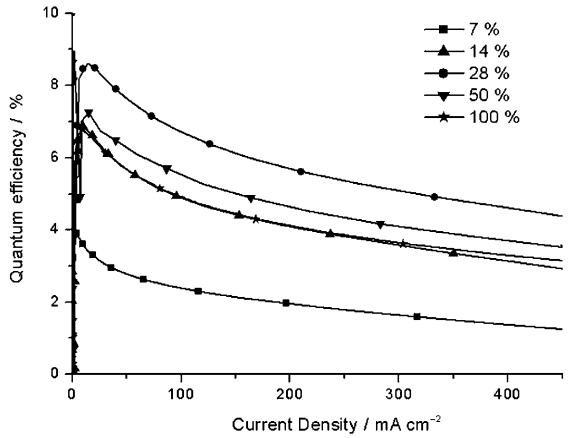

Figure 11. Quantum efficiency of OLED devices ITO/NPB/mCP/TPSi-F:**1**/BCP/TPBI/LiF/Al as a function of dopant concentration.

1 cd m^{-2}) and maximum external quantum efficiency (EQE) of 8.62 at 11.5 V, CIE coordinates of (0.53, 0.46) at 8 V, and maximum brightness of 47543 cd m^{-2} at a driving voltage of 18.5 V. At higher dopant concentrations, the EQE decreases, probably arising from triplet–triplet annihilation.[15a] Its performance data are nevertheless very encouraging, showing characteristics comparable to the best Pt^{II}-based OLEDs documented in literature,[34] and giving a peak η_{ext} of 8.5% (corresponding to a luminance efficiency of 18.5 cd A^{-1}), together with a brightness of 3700 cd m^{-2} at a current density of 20 mA cm^{-2}. Even at a higher current density of 100 mA cm^{-2}, 80% of the peak efficiency (6.7%) could still be sustained, together with a fairly bright phosphorescence of approximately 14570 cd m^{-2}. We attribute this superiority to the higher emission QE and its shorter triplet lifetime. The latter helped to minimize the degree of exciton quenching through triplet–triplet annihilation occurring at high current density.

Conclusions

In summary, facile syntheses are established for Pt^{II} complexes that possess the common terdentate chelating anion fpbpy and a monodentate anion occupying the fourth coordination site. From structural and spectroscopic characterization, it is demonstrated that the inter-conversion between the chloride complex **1** and the acetamide complexes **3** and **4** can be achieved by organonitrile coordination, base-induced organonitrile hydrolysis, and release of the respective acetamide ligand by addition of HCl. In dilute solution, complexes **1**, **2**, and **3** exhibit orange (560 nm), orange (557 nm), and red (604 nm) phosphorescence, respectively, in which complexes **1** and **2** show strong concentration-dependent emission originating from the excimeric type association in the excited state, which is manifested in a strong Pt–Pt interaction. For complex **1**, the moderately strong deep-red emission with quantum yield of ~0.2 and short lifetime of ~113 ns may find useful application in the field of red-emitting OLEDs. Work focusing on this aspect is currently in progress.

Experimental Section

General Information and Materials

All reactions were performed under a nitrogen atmosphere using anhydrous solvents or solvents treated with an appropriate drying reagent. Mass spectra were obtained on a JEOL SX-102 A instrument operating in electron-impact (EI) mode or fast-atom-bombardment (FAB) mode. ^{1}H and ^{19}F NMR spectra were recorded on Varian Mercury-400 or INOVA-500 instruments. Elemental analyses were conducted at the NSC Regional Instrumentation Center at National Chiao Tung University.

Steady-state absorption and emission spectra were recorded by a Hitachi (U-3310) spectrophotometer and an Edinburgh (FS920) fluorimeter, respectively. Solution samples, unless otherwise specified, were degassed by three freeze-pump-thaw cycles. A confocal microscope (Witec α SNOM) connected with an intensified charge-coupled detector (PI-MAX) by the optical fiber was used to measure the emission spectra of single crystal samples. Coumarin 480 ($\Phi = 0.93$ in EtOH)[35] was used as a reference to determine the luminescence quantum yields of the studied compounds in solution, using Equation (7):

$$\Phi_s = \Phi_r \left(\frac{\eta_s^2 A_r I_s}{\eta_r^2 A_s I_r} \right) \quad (7)$$

in which Φ_s and Φ_r are the quantum yields of the unknown and reference samples, respectively, η is the refractive index of the solvent, A_r and A_s are the absorbance of the reference and the unknown samples at the excitation wavelength, and I_s and I_r are the integrated areas under the emission spectra of interest, respectively. An integrating sphere (Lab sphere) was applied to measure the quantum yield in the solid state. The solid thin film was prepared by direct vacuum deposition and was excited by an argon-ion laser at 363 nm. The resulting luminescence was acquired with an intensified charge-coupled detector for subsequent quantum yield analyses according to a reported method.[36]

Synthesis

Pt(fpbpy)Cl (**1**) (Method A): A mixture of K_2PtCl_4 (300 mg, 0.72 mmol) and 6-(5-trifluoromethyl-pyrazol-3-yl)-2,2′-bipyridine (fpbpyH) (210 mg, 0.72 mmol) in a 1:1 mixture of water and acetonitrile (30 mL) was vigorously refluxed for 48 h, giving a red-violet precipitate. After cooling the suspension to room temperature, the precipitate (**1**, 319 mg, 0.61 mmol, 85%) was filtered, washed with diethyl ether, and dried under vacuum. X-ray crystals were afforded by cooling the saturated solution of **1** in a 1:3 mixture of DMSO and acetone.

(**1**) (Method B): To a suspension of Pt(fpbpy)(NHCOMe) (**3**) (40 mg, 0.071 mmol) in a 3:1 mixture of acetonitrile and water (20 mL), was added a small amount of HCl (2 M) to afford a clear solution. The solution was refluxed for 6 h, giving a red-violet suspension. After cooling to room temperature, the precipitate (**1**, 32 mg, 0.061 mmol, 86%) was filtered, washed with diethyl ether, and dried under vacuum.

Spectral data of **1**: ^{1}H NMR (400 MHz, [D$_6$]DMSO, 298 K, TMS): $\delta =$ 8.95 (d, $J_{H,H} = 5.6$ Hz, 1H), 8.49 (d, $J_{H,H} = 7.6$ Hz, 1H), 8.39 (td, $J_{H,H} = 7.8$, 1.6 Hz, 1H), 8.30–8.22 (m, 2H), 7.99 (dd, $J_{H,H} = 7.6$, 1.2 Hz, 1H), 7.86 (td, $J_{H,H} = 6.6$, 1.3 Hz, 1H), 7.29 ppm (s, 1H); ^{19}F NMR (470 MHz, [D$_7$]DMF, 298 K): $\delta = -60.47$ ppm (s, 3F, CF_3); MS (FAB, ^{195}Pt): m/z (%) calcd for $C_{14}H_8ClF_3N_4Pt$: 519.00 $[M]^+$; found: 519.00; elemental analysis: calcd (%) for $C_{14}H_8ClF_3N_4Pt$: C 32.35, H 1.55, N 10.78; found: C 32.44, H 1.74, N 10.32.

Pt(fpbpy)(OAc) (**2**): A mixture of **1** (50 mg, 0.096 mmol) and silver acetate (65 mg, 0.389 mmol) in DMF (15 mL) was stirred at 110 °C for 50 min to give an orange suspension. After cooling to room temperature, the solution was filtered, the filtrate was concentrated under vacuum, and the residue was dissolved in a small amount of DMF. Large excess of diethyl ether was added to induce the precipitation. The orange precipi-

tate (**2**, 42 mg, 0.077 mmol, 80%) was collected, washed with diethyl ether, and dried under vacuum.

Spectral data of **2**: ^{1}H NMR (500 MHz, [D$_6$]DMSO, 298 K, TMS): $\delta =$ 8.51 (d, $J_{H,H} = 8.0$ Hz, 1H), 8.49 (d, $J_{H,H} = 5.0$ Hz, 1H), 8.42 (td, $J_{H,H} = 7.9$, 1.3 Hz, 1H), 8.28 (t, $J_{H,H} = 8.0$ Hz, 1H), 8.22 (d, $J_{H,H} = 7.8$ Hz, 1H), 7.99 (d, $J_{H,H} = 7.5$ Hz, 1H), 7.86 (td, $J_{H,H} = 6.9$, 1.5 Hz, 1H), 7.30 (s, 1H), 2.05 ppm (s, 3H); ^{19}F NMR (470 MHz, [D$_6$]DMSO, 298 K): $\delta =$ −59.23 ppm (s, 3F, CF_3); MS (FAB, ^{195}Pt): *m*/*z* (%) calcd for $C_{16}H_{11}F_3N_4O_2Pt$: 544.05 $[M+1]^+$; found: 544.00; elemental analysis: calcd (%) for $C_{16}H_{11}F_3N_4O_2Pt$: C 35.37, H 2.04, N 10.31; found: C 34.94, H 2.37, N 10.59.

Pt(fpbpy)(NHCOMe) (**3**) (Method A): A mixture of **1** (50 mg, 0.096 mmol), acetamide (57 mg, 0.965 mmol), and Na_2CO_3 (102 mg, 0.962 mmol) in ethanol (30 mL) was refluxed overnight. After cooling to room temperature, the solvent was removed under vacuum, and the residue was dissolved in a small amount of DMF. The crystalline product (3, 39 mg, 0.072 mmol, 75%) was recrystallized from a mixture of DMF and diethyl ether. Single crystals suitable for X-ray diffraction analysis were obtained by placing the saturated solution of **3** in DMSO at room temperature for several days.

(**3**) (Method B): A mixture of **1** (60 mg, 0.116 mmol) and Na_2CO_3 (13 mg, 0.123 mmol) in a 1:1 mixture of water and acetonitrile (20 mL) was refluxed overnight, giving a yellow precipitate. After cooling the suspension to room temperature, the precipitate (3, 60 mg, 0.107 mmol, 92%) was filtered, washed with diethyl ether, and then dried under vacuum.

(**3**) (Method C): A mixture of **5** (55 mg, 0.090 mmol) and Na_2CO_3 (13 mg, 0.123 mmol) in a 3:1 mixture of acetonitrile and water (20 mL) was refluxed overnight, giving a yellow precipitate. After cooling the suspension to room temperature, the precipitate (3, 42 mg, 0.075 mmol, 83%) was filtered, washed with diethyl ether, and dried under vacuum.

Spectral data of **3**: ^{1}H NMR (400 MHz, [D$_6$]DMSO, 298 K, TMS): $\delta =$ 9.48 (d, $J_{H,H} = 5.0$ Hz, 1H), 8.42 (d, $J_{H,H} = 7.6$ Hz, 1H), 8.30 (td, $J_{H,H} = 7.8$, 1.6 Hz, 1H), 8.22–8.15 (m, 2H), 7.91 (dd, $J_{H,H} = 5.8$, 3.0 Hz, 1H), 7.70 (td, $J_{H,H} = 6.7$, 1.5 Hz, 1H), 7.25 (s, 1H), 5.58 (s, 1H), 2.00 ppm (s, 3H); ^{19}F NMR (470 MHz, [D$_7$]DMF, 298 K): $\delta = -60.33$ (s, 3F, CF_3); MS (FAB, ^{195}Pt): *m*/*z* (%) calcd for $C_{16}H_{12}F_3N_5OPt$: 542.06 $[M]^+$; found: 542.00; elemental analysis: calcd (%) for $C_{16}H_{12}F_3N_5OPt \cdot H_2O$: C 34.29, H 2.52, N 12.50; found: C 34.24, H 2.78, N 12.21.

Pt(fpbpy)(NHCOEt) (**4**): A mixture of **1** (41 mg, 0.079 mmol), propionamide (91 mg, 1.245 mmol), and Na_2CO_3 (150 mg, 1.415 mmol) in ethanol (15 mL) was refluxed for 24 h, and then cooled to room temperature. The solvents and excess propionamide were removed under vacuum, and the residue was dissolved in small amount of DMF. Large excess of water was added to induce precipitation. The yellow precipitate was collected, washed with diethyl ether, and dried under vacuum. The crystalline product (**4**, 19 mg, 0.034 mmol, 43%) was obtained from a mixture of DMF and diethyl ether.

Spectral data of **4**: ^{1}H NMR (500 MHz, [D$_6$]DMSO, 298 K, TMS): $\delta = 9.75$ (d, $J_{H,H} = 5.0$ Hz, 1H), 8.48 (d, $J_{H,H} = 7.5$ Hz, 1H), 8.36 (td, $J_{H,H} = 7.9$, 1.3 Hz, 1H), 8.27–8.23 (m, 2H), 7.98 (dd, $J_{H,H} = 6.0$, 2.5 Hz, 1H), 7.77 (td, $J_{H,H} = 6.8$, 1.5 Hz, 1H), 7.32 (s, 1H), 5.60 (s, 1H), 2.28 (q, $J_{H,H} = 7.5$ Hz, 2H), 1.08 ppm (t, $J_{H,H} = 7.3$ Hz, 3H). ^{19}F NMR (470 MHz, [D$_6$]DMSO, 298 K): $\delta = -59.24$ ppm (s, 3F, CF_3); MS (FAB, ^{195}Pt): *m*/*z* (%) calcd for $C_{17}H_{14}F_3N_5OPt$: 557.08 $[M+1]^+$; found: 557.00; elemental analysis: calcd (%) for $C_{17}H_{14}F_3N_5OPt \cdot H_2O$: C 35.55, H 2.81, N 12.19; found: C 35.47, H 3.08, N 12.11.

[Pt(fpbpy)(NCMe)](BF$_4$) (**5**): A mixture of **1** (60 mg, 0.115 mmol) and $AgBF_4$ (23 mg, 0.118 mmol) in anhydrous acetonitrile (15 mL) was refluxed for 4 h to give a yellow suspension. The solution was filtered and the filtrate was concentrated to approximately 3 mL. Yellow crystalline material (5, 57 mg, 0.093 mmol, 80%)was obtained by a slow diffusion of diethyl ether into the acetonitrile solution.

Spectral data of **5**: ^{1}H NMR (400 MHz, [D$_6$]DMSO, 298 K, TMS): $\delta =$ 9.24 (d, $J_{H,H} = 5.6$ Hz, 1H), 8.68 (d, $J_{H,H} = 8.0$ Hz, 1H), 8.57–8.46 (m, 3H), 8.23 (d, $J_{H,H} = 7.6$ Hz, 1H), 8.05 (t, $J_{H,H} = 6.8$ Hz, 1H), 7.54 (s, 1H), 2.06 ppm (s, 3H); ^{19}F NMR (470 MHz, [D$_6$]DMSO, 298 K): $\delta = -60.09$ (s, 3F, CF_3), −148.22 ppm (s, 4F, BF_4^-); MS (FAB, ^{195}Pt): *m*/*z* (%) calcd for $C_{16}H_{11}F_3N_5Pt$: 525.06 $[M\text{-}BF_4]^+$; found: 525.00; elemental analysis: calcd (%) for $C_{16}H_{11}BF_7N_5Pt \cdot 2H_2O$: C 29.65, H 2.33, N 10.80; found: C 29.92, H 2.30, N 10.60.

X-ray Diffraction Studies

Single crystal X-ray diffraction data of **1** and **3** were measured on a Bruker SMART Apex CCD diffractometer using ($Mo_{K\alpha}$) radiation ($\lambda =$ 0.71073 Å). The data collection was executed using the SMART program. Cell refinement and data reduction were performed with the SAINT program. The structure was determined using the SHELXTL/PC program and refined using full-matrix least squares. Their crystallographic refinement parameters are summarized in Table 5. CCDC 93182 and 693183 contain the supplementary crystallographic data for this paper. These data can be obtained free of charge from The Cambridge Crystallographic Data Centre at www.ccdc.cam.ac.uk/data_request/cif.

DFT Calculation Method

Molecular orbital and time-dependent calculations are based on the structures from the X-ray crystal studies at B3LYP level in the continuum solvation model of CH_2Cl_2 (IEFPCM). The basis set is a double-ζ quality basis set consisting of Hay and Wadt's quasi-relativistic effective core potentials (LANL2DZ) for Pt^{II} atom;[37] a 6-31G* basis set was employed for the H, C, N, F, and O atoms. Typically, the lowest three triplet and singlet roots of the nonhermitian eigenvalue equations were obtained to determine the vertical excitation energies. Oscillator strengths were de-

Table 5. Crystal data and refinement parameters for complexes **1** and **3**.

	1	**3**
Empirical formula	$C_{17}H_{14}ClF_3N_4OPt$	$C_{18}H_{18}F_3N_5O_2PtS$
Formula weight	577.86	620.52
Temperature [K]	150(2)	220(2)
Crystal system	Monoclinic	Triclinic
Space group	$P2_1/m$	$P\bar{1}$
a [Å]	9.3098(7)	7.8258(5)
b [Å]	6.5917(5)	13.7404(8)
c [Å]	15.1612(11)	19.1996(11)
α [°]		87.338(1)
β [°]	106.399(2)	78.825(1)
γ [°]		88.222(1)
V [Å^3]	892.55(12)	2022.7(2)
Z	2	4
ρ_{calcd} [g cm^{-3}]	2.150	2.038
μ [mm^{-1}]	8.055	7.093
F(000)	548	1192
Crystal size [mm^3]	0.20 × 0.15 × 0.02	0.40 × 0.12 × 0.07
Reflns. collected	5436	21419
Independent reflections	1713 [*R*(int) = 0.0459]	9241 [*R*(int) = 0.0418]
Max., min. transmission	0.8555, 0.2957	0.6366, 0.1636
Data/restraints/parameters	1713/0/168	9241/0/548
GOF	1.202	1.088
Final *R* indices [$I > 2\sigma(I)$]	$R_1 = 0.0401$, $wR_2 = 0.0918$	$R_1 = 0.0456$, $wR_2 = 0.0956$
R indices (all data)	$R_1 = 0.0428$, $wR_2 = 0.0930$	$R_1 = 0.0601$, $wR_2 = 0.1093$
Largest different peak and hole	4.946 and −2.156 e Å^{-3}	2.653 and −1.416 e Å^{-3}

duced from the dipole-transition matrix elements (for singlet states only). All the calculations were performed with the Gaussian 03 package.[38] Compositions of molecular orbitals, overlap populations between molecular fragments, and density-of-states spectra were calculated using the AOMix program.[39]

Fabrication of Light-Emitting Devices

The EL devices were fabricated by vacuum deposition of the materials at 10^{-6} Torr onto a clean glass that was pre-coated with a layer of indium tin oxide with a sheet resistance of 25 Ω square^{-1}. Various organic layers were deposited sequentially at a rate of 1–2 Å s^{-1}. Phosphorescent dopant was co-evaporated with TPSi-F by two independent sources. A thin layer of LiF (1 nm) and a thick layer of Al (150 nm) were sequentially deposited as the cathode. The active area of the emitting diode was 9.00 mm^2. The current-voltage-luminance of the devices was measured in ambient conditions with a Keithley 2400 Source meter and a Newport 1835C Optical meter equipped with an 818ST silicon photodiode. The EL spectrum was obtained using a Hitachi F4500 spectrofluorimeter.

Acknowledgements

This work was supported by the National Science Council and Ministry of Economic Affairs of Taiwan.

[1] a) F. Guo, W. Sun, Y. Liu, K. Schanze, *Inorg. Chem.* **2005**, *44*, 4055; b) R. Vestberg, R. Westlund, A. Eriksson, C. Lopes, M. Carlsson, B. Eliasson, E. Glimsdal, M. Lindgren, E. Malmström, *Macromolecules* **2006**, *39*, 2238; c) P. Lind, D. Boström, M. Carlsson, A. Eriksson, E. Glimsdal, M. Lindgren, B. Eliasson, *J. Phys. Chem. A* **2007**, *111*, 1598.

[2] a) S. C. F. Kui, I. H. T. Sham, C. C. C. Cheung, C.-W. Ma, B. Yan, N. Zhu, C.- M. Che, F.-H. Fu, *Chem. Eur. J.* **2007**, *13*, 417; b) J. A. G. Williams, *Top. Curr. Chem.* **2007**, *281*, 205.

[3] a) M. Albrecht, M. Lutz, A. L. Spek, G. van Koten, *Nature* **2000**, *406*, 970; b) S. C. F. Kui, S. S.-Y. Chui, C.- M. Che, N. Zhu, *J. Am. Chem. Soc.* **2006**, *128*, 8297.

[4] D.-L. Ma, T. Y.-T. Shum, F. Zhang, C.-M. Che, M. Yang, *Chem. Commun.* **2005**, 4675.

[5] a) D. Zhang, L.-Z. Wu, L. Zhou, X. Han, Q.-Z. Yang, L.-P. Zhang, C.-H. Tung, *J. Am. Chem. Soc.* **2004**, *126*, 3440; b) K. Feng, R.-Y. Zhang, L.-Z. Wu, B. Tu, M.- L. Peng, L.-P. Zhang, D. Zhao, C.-H. Tung, *J. Am. Chem. Soc.* **2006**, *128*, 14685.

[6] F. N. Castellano, I. E. Pomestchenko, E. Shikhova, F. Hua, M. L. Muro, N. Rajapakse, *Coord. Chem. Rev.* **2006**, *250*, 1819.

[7] a) W. Lu, M. C. W. Chan, N. Zhu, C.-M. Che, C. Li, Z. Hui, *J. Am. Chem. Soc.* **2004**, *126*, 7639; b) C. Yu, K. M.-C. Wong, K. H.-Y. Chan, V. W.-W. Yam, *Angew. Chem.* **2005**, *117*, 801; *Angew. Chem. Int. Ed.* **2005**, *44*, 791; c) B. Ma, J. Li, P. I. Djurovich, M. Yousufuddin, R. Bau, M. E. Thompson, *J. Am. Chem. Soc.* **2005**, *127*, 28.

[8] C. N. Pettijohn, E. B. Jochnowitz, B. Chuong, J. K. Nagel, A. Vogler, *Coord. Chem. Rev.* **1998**, *171*, 85.

[9] a) S. W. Thomas III, K. Venkatesan, P. Müller, T. M. Swager, *J. Am. Chem. Soc.* **2006**, *128*, 16641; b) N. M. Shavaleev, H. Adams, J. Best, R. Edge, S. Navaratnam, J. A. Weinstein, *Inorg. Chem.* **2006**, *45*, 9410; c) D. E. Janzen, L. F. Mehne, D. G. VanDerveer, G. J. Grant, *Inorg. Chem.* **2005**, *44*, 8182.

[10] W. R. Browne, C. M. O'Connor, H. P. Hughes, R. Hage, O. Walter, M. Doering, J. F. Gallagher, J. G. Vos, *J. Chem. Soc. Dalton Trans.* **2002**, 4048.

[11] P.-T. Chou, Y. Chi, *Chem. Eur. J.* **2007**, *13*, 380.

[12] a) Y. Chi, P.-T. Chou, *Chem. Soc. Rev.* **2007**, *36*, 1421; b) P.-T. Chou, Y. Chi, *Eur. J. Inorg. Chem.* **2006**, 3319.

[13] a) S.-W. Lai, M. C.-W. Chan, K.-K. Cheung, C.-M. Che, *Organometallics* **1999**, *18*, 3327; b) W. Lu, B.-X. Mi, M. C. W. Chan, Z. Hui, C.-M. Che, N. Zhu, S.-T. Lee, *J. Am. Chem. Soc.* **2004**, *126*, 4958; c) W. Sun, H. Zhu, P. M. Barron, *Chem. Mater.* **2006**, *18*, 2602.

[14] a) D. J. Cárdenas, A. M. Echavarren, M. C. Ramírez de Arellano, *Organometallics* **1999**, *18*, 3337; b) J. A. G. Williams, A. Beeby, E. S. Davies, J. A. Weinstein, C. Wilson, *Inorg. Chem.* **2003**, *42*, 8609; c) B. Soro, S. Stoccoro, G. Minghetti, A. Zucca, M. A. Cinellu, M. Manassero, S. Gladiali, *Inorg. Chim. Acta* **2006**, *359*, 1879.

[15] a) J. Kavitha, S.-Y. Chang, Y. Chi, J.- K. Yu, Y.-H. Hu, P.-T. Chou, S.-M. Peng, G.-H. Lee, Y.-T. Tao, C.-H. Chien, A. J. Carty, *Adv. Funct. Mater.* **2005**, *15*, 223; b) S.-Y. Chang, J. Kavitha, S.-W. Li, C.-S. Hsu, Y. Chi, Y.-S. Yeh, P.-T. Chou, G.-H. Lee, A. J. Carty, Y.-T. Tao, C.-H. Chien, *Inorg. Chem.* **2006**, *45*, 137.

[16] Y.-H. Song, Y.-C. Chiu, Y. Chi, P.-T. Chou, Y.-M. Cheng, C.-W. Lin, G.-H. Lee, A. J. Carty, *Organometallics* **2008**, *27*, 80.

[17] a) C. M. Jensen, W. C. Trogler, *J. Am. Chem. Soc.* **1986**, *108*, 723; b) T. Ghaffar, A. W. Parkins, *Tetrahedron Lett.* **1995**, *36*, 8657; c) X.-B. Jiang, A. J. Minnaard, B. L. Feringa, J. G. de Vries, *J. Org. Chem.* **2004**, *69*, 2327.

[18] a) K. Chen, Y.-M. Cheng, Y. Chi, M.-L. Ho, C.-H. Lai, P.-T. Chou, S.-M. Peng, G.-H. Lee, *Chem. Asian J.* **2007**, *2*, 155; b) K.-S. Chen, W.-H. Liu, Y.-H. Wang, C.-H. Lai, P.-T. Chou, G.-H. Lee, K. Chen, H.-Y. Chen, Y. Chi, F.-C. Tung, *Adv. Funct. Mater.* **2007**, *17*, 2964.

[19] a) S.-Y. Chang, J. Kavitha, J.-Y. Hung, Y. Chi, Y.-M. Cheng, E. Y. Li, P.-T. Chou, G.-H. Lee, A. J. Carty, *Inorg. Chem.* **2007**, *46*, 7064; b) S.-Y. Chang, J.-L. Chen, Y. Chi, Y.-M. Cheng, G.-H. Lee, C.-M. Jiang, P.-T. Chou, *Inorg. Chem.* **2007**, *46*, 11202.

[20] a) M. Albrecht, R. A. Gossage, M. Lutz, A. L. Spek, G. van Koten, *Chem. Eur. J.* **2000**, *6*, 1431; b) S.-W. Lai, M. C.-W. Chan, T.-C. Cheung, S.-M. Peng, C.-M. Che, *Inorg. Chem.* **1999**, *38*, 4046; c) K. J. H. Young, S. K. Meier, J. M. Gonzales, J. Oxgaard, W. A. Goddard III, R. A. Periana, *Organometallics* **2006**, *25*, 4734; d) C.-K. Koo, B. Lam, S.-K. Leung, M. H.-W. Lam, W.-Y. Wong, *J. Am. Chem. Soc.* **2006**, *128*, 16434; e) A. Hofmann, L. Dahlenburg, R. van Eldik, *Inorg. Chem.* **2003**, *42*, 6528.

[21] a) V. W.-W. Yam, R. P.-L. Tang, K. M.-C. Wong, K.-K. Cheung, *Organometallics* **2001**, *20*, 4476; b) R. Büchner, J. S. Field, R. J. Haines, C. T. Cunningham, D. R. Mcmillin, *Inorg. Chem.* **1997**, *36*, 3952.

[22] a) J. A. Bailey, M. G. H. Hill, R. E. Marsh, V. M. Miskowski, W. P. Schaefer, H. B. Gray, *Inorg. Chem.* **1995**, *34*, 4591; b) C.-K. Koo, Y.-M. Ho, C.-F. Chow, M. H.-W. Lam, T.-C. Lau, W.-Y. Wong, *Inorg. Chem.* **2007**, *46*, 3603.

[23] a) V. W.-W. Yam, K. M.-C. Wong, N. Zhu, *J. Am. Chem. Soc.* **2002**, *124*, 6506; b) Y. Sun, K. Ye, H. Zhang, J. Zhang, L. Zhao, B. Li, G. Yang, B. Yang, Y. Wang, S.-W. Lai, C.-M. Che, *Angew. Chem.* **2006**, *118*, 5687; *Angew. Chem. Int. Ed.* **2006**, *45*, 5561.

[24] W. Chen, F. Liu, D. Xu, K. Matsumoto, S. Kishi, M. Kato, *Inorg. Chem.* **2006**, *45*, 5552.

[25] a) K. M.-C. Wong, N. Zhu, V. W.-W. Yam, *Chem. Commun.* **2006**, 3441; b) E. J. Ziolkowski, P. Turner, L. M. Rendina, *Inorg. Chem. Commun.* **2006**, *9*, 53; c) K. Uemura, K. Fukui, H. Nishikawa, S. Arai, K. Matsumoto, H. Oshio, *Angew. Chem.* **2005**, *117*, 5595; *Angew. Chem. Int. Ed.* **2005**, *44*, 5459.

[26] a) T. J. Wadas, Q.- M. Wang, Y.-J. Kim, C. Flaschenreim, T. N. Blanton, R. Eisenberg, *J. Am. Chem. Soc.* **2004**, *126*, 16841; b) C. E. Buss, K. R. Mann, *J. Am. Chem. Soc.* **2002**, *124*, 1031.

[27] C. A. Hunter, M. N. Meah, J. K. M. Sanders, *J. Am. Chem. Soc.* **1990**, *112*, 5773.

[28] a) D. J. Tozer, R. D. Amos, N. C. Handy, B. O. Roos, L. Serrano-Andrés, *Mol. Phys.* **1999**, *97*, 859; b) J. Fabian, *Theor. Chem. Acc.* **2001**, *106*, 199; c) Z.-L. Cai, K. Sendt, J. R. Reimers, *J. Chem. Phys.* **2002**, *117*, 5543; d) M.-S. Liao, Y. Lu, S. Scheiner, *J. Comput. Chem.* **2003**, *24*, 623; e) A. Dreuw, J. L. Weisman, M. Head-Gordon, *J. Chem. Phys.* **2003**, *119*, 2943; f) S. Grimme, M. Parac, *ChemPhysChem* **2003**, *4*, 292; g) A. L. Sobolewski, W. Domcke, *Chem. Phys.* **2003**, *294*, 73; h) A. Dreuw, G. R. Fleming, M. Head-Gordon, *J. Phys. Chem. B* **2003**, *107*, 6500; i) M. Lundberg, P. E. M. Siegbahn, *J. Chem. Phys.* **2005**, *122*, 224103.

[29] C.-K. Koo, B. Lam, S.-K. Leung, M. H.-W. Lam, W.-Y. Wong, *J. Am. Chem. Soc.* **2006**, *128*, 16434.

[30] P.-I. Shih, C.-H. Chien, C.-Y. Chuang, C.-F. Shu, C.-H. Yang, J.-H. Chen, Y. Chi, *J. Mater. Chem.* **2007**, *17*, 1692.

[31] a) Y.-L. Tung, L.-S. Chen, Y. Chi, S.-W. Lee, P.-T. Chou, Y.-M. Cheng, E. Y. Li, G.-H. Lee, C.-F. Shu, F.-I. Wu, A. J. Carty, *Adv. Funct. Mater.* **2006**, *16*, 1615; b) Y.-L. Tung, S.-W. Lee, Y. Chi, L.-S. Chen, C.-F. Shu, F.-I. Wu, A. J. Carty, P.-T. Chou, S.-M. Peng, G.-H. Lee, *Adv. Mater.* **2005**, *17*, 1059; c) P.-I. Shih, C.-H. Chien, F.-I. Wu, C.-F. Shu, *Adv. Funct. Mater.* **2007**, *17*, 3514.

[32] M. Hissler, J. E. McGarrah, W. B. Connick, D. K. Geiger, S. Cummings, *Coord. Chem. Rev.* **2000**, *208*, 115.

[33] a) B. W. D′Andrade, S. R. Forrest, *Adv. Mater.* **2004**, *16*, 1585; b) B. W. D′Andrade, J. Brooks, V. Adamovich, M. E. Thompson, S. R. Forrest, *Adv. Mater.* **2002**, *14*, 1032; c) H. F. Xiang, S. C. Chan, K. K. Y. Wu, C. M. Che, P. T. Lai, *Chem. Commun.* **2005**. 1408.

[34] a) R. C. Kwong, S. Sibley, T. Dubovoy, M. Baldo, S. R. Forrest, M. E. Thompson, *Chem. Mater.* **1999**, *11*, 3709; b) C. M. Che, Y. J. Hou, M. C. W. Chan, J. Guo, Y. Liu, Y. Wang, *J. Mater. Chem.* **2003**, *13*, 1362; c) Y. H. Song, S. J. Yeh, C. T. Chen, Y. Chi, C. S. Liu, J. K. Yu, Y. H. Hu, P. T. Chou, S. M. Peng, G. H. Lee, *Adv. Funct. Mater.* **2004**, *14*, 1221.

[35] G. Jones II, W. R. Jackson, A. M. Halpern, *Chem. Phys. Lett.* **1980**, *72*, 391.

[36] J. C. de Mello, H. F. Wittmann, R. H. Friend, *Adv. Mater.* **1997**, *9*, 230.

[37] a) P. J. Hay, R. W. Wadt, *J. Chem. Phys.* **1985**, *82*, 270; b) W. R. Wadt, P. J. Hay, *J. Chem. Phys.* **1985**, *82*, 284; c) P. J. Hay, W. R. Wadt, *J. Chem. Phys.* **1985**, *82*, 299.

[38] Gaussian 03 (Revision C.02), M. J. Frisch, G. W. Trucks, H. B. Schlegel, G. E. Scuseria, M. A. Robb, J. R. Cheeseman, J. A. Montgomery, Jr., T. Vreven, K. N. Kudin, J. C. Burant, J. M. Millam, S. S. Iyengar, J. Tomasi, V. Barone, B. Mennucci, M. Cossi, G. Scalmani, N. Rega, G. A. Petersson, H. Nakatsuji, M. Hada, M. Ehara, K. Toyota, R. Fukuda, J. Hasegawa, M. Ishida, T. Nakajima, Y. Honda, O. Kitao, H. Nakai, M. Klene, X. Li, J. E. Knox, H. P. Hratchian, J. B. Cross, V. Bakken, C. Adamo, J. Jaramillo, R. Gomperts, R. E. Stratmann, O. Yazyev, A. J. Austin, R. Cammi, C. Pomelli, J. W. Ochterski, P. Y. Ayala, K. Morokuma, G. A. Voth, P. Salvador, J. J. Dannenberg, V. G. Zakrzewski, S. Dapprich, A. D. Daniels, M. C. Strain, O. Farkas, D. K. Malick, A. D. Rabuck, K. Raghavachari, J. B. Foresman, J. V. Ortiz, Q. Cui, A. G. Baboul, S. Clifford, J. Cioslowski, B. B. Stefanov, G. Liu, A. Liashenko, P. Piskorz, I. Komaromi, R. L. Martin, D. J. Fox, T. Keith, M. A. Al-Laham, C. Y. Peng, A. Nanayakkara, M. Challacombe, P. M. W. Gill, B. Johnson, W. Chen, M. W. Wong, C. Gonzalez, J. A. Pople, Gaussian, Inc., Wallingford, CT, **2004**.

[39] a) S. I. Gorelsky, *AOMix: Program for Molecular Orbital Analysis*, http://www.sg-chem.net/, University of Ottawa, **2007**; b) S. I. Gorelsky, A. B. P. Lever, *J. Organomet. Chem.* **2001**, *635*, 187.

Received: May 21, 2008
Published online: September 2, 2008

